Comparison of siliconatom diffusion on the dimer–adatomstacking fault and Binnig e t a l. models of the reconstructed Si(111)(7×7) surface

Paras M. Agrawal, Donald L. Thompson, and Lionel M. Raff

Citation: The Journal of Chemical Physics **94**, 6243 (1991); doi: 10.1063/1.460413
View online: http://dx.doi.org/10.1063/1.460413
View Table of Contents: http://scitation.aip.org/content/aip/journal/jcp/94/9?ver=pdfcov
Published by the AIP Publishing

Comparison of silicon-atom diffusion on the dimer–adatom-stacking fault and Binnig *et al.* models of the reconstructed Si(111)-(7×7) surface

Paras M. Agrawal, Donald L. Thompson, and Lionel M. Raff
Department of Chemistry, Oklahoma State University, Stillwater, Oklahoma 74078

(Received 8 November 1990; accepted 22 January 1991)

The dynamics of silicon-atom diffusion on the dimer–adatom-stacking fault model (DAS) of the reconstructed Si(111)-(7×7) surface suggested by Takayanagi *et al.* have been investigated using variational phase-space theory methods. The site-to-site jump frequency is obtained from the variationally minimized total flux across a right cylindrical dividing surface whose cross section in the surface plane is formed from straight line and elliptical segments. This minimized flux is corrected for surface recrossings by the computation of trajectories starting from phase-space points in the transition-state region that are obtained in the Markov walk used to evaluate the phase-space integrals in the expression for the total classical flux. The jump frequencies are used as input to the set of differential equations that describes the diffusion rates on the DAS surface. Values of the diffusion coefficient D are computed from the slopes of plots of the time variation of the root-mean-square displacements obtained from the solution of the rate equations. Arrhenius plots of the results at 300, 600, and 1000 K yield $D = 0.124 \exp[-2.18\ \text{eV/kT}]\ \text{cm}^2/\text{s}$. These rates are orders of magnitude smaller than the corresponding rates we have previously obtained for silicon-adatom diffusion on the Binnig *et al.* model of the Si(111)-(7×7) surface. In addition, it is found that the diffusion pattern on the DAS surface is uniform with no preferential directions for silicon-atom flow. In contrast, diffusion on the Binnig surface was found to occur via gateways at three of the four corners of the unit cell. This led to preferential directions for adatom flow. These differences lead us to suggest that careful measurements of silicon-adatom diffusion rates on the Si(111)-(7×7) surface may be a very sensitive measure of the extent to which these surface models accurately describe the experimental Si(111)-(7×7) reconstruction.

I. INTRODUCTION

It is well known that the atomic structure of a silicon surface differs from that of an ideal truncated lattice due to reconstruction of the surface. One of the most interesting silicon surfaces is the (111) plane as three different phases of reconstruction have been observed for this crystal plane: (a) a vacuum-cleaved metastable (2×1) surface, (b) a (1×1) phase which is stable only at temperatures higher than 1300 K, and (c) an annealed (7×7) surface which is the thermodynamically most stable phase near room temperature.

Several models of the Si(111)-(7×7) reconstruction have been suggested. These include a buckled ring model by Chadi *et al.*,[1-3] adatom models suggested by Harrison,[4] Binnig *et al.*,[5] and Chadi,[1-3] a pyramidal cluster model by Aono *et al.*,[6] a modified milkstool model by Snyder,[7] stacking-fault models proposed by Bennett *et al.*,[8] McRae,[9] and Himpsel and Batra,[10,11] and a dimer–adatom-stacking fault (DAS) model proposed by Takayanagi *et al.*[12] Each of these models has recently been reviewed by Tromp and van Loenen.[13] Tromp[14] and Yamaguchi[15] have used Keating-type[16] expressions for the lattice potential and have obtained the relaxed equilibrium configurations for several of these proposed models.

At present, it is not completely clear which of the above models most nearly corresponds to the actual (7×7) surface. The available experimental evidence is equivocal.[5,6] In this paper, we present theoretical evidence that careful measurement of silicon-atom diffusion rates, activation energies, and diffusion patterns may be one of the most sensitive measures of the actual structure of the (7×7) lattice.

We have recently reported variational phase-space theory studies of silicon-atom diffusion rates and patterns on the Binnig *et al.*[5] model of the (7×7) reconstruction using a modified Keating potential[16] to describe the lattice interactions.[17] The results gave an activation energy for silicon-atom surface diffusion of 34.8 kcal/mol and a frequency factor of $2.15\times10^{-3}\ \text{cm}^2/\text{s}$. Surface diffusion was found to be nonisotropic, occurring via "gateways" at three of the four corners of the (7×7) unit cell.

In the present work, we report the results of similar calculations using the DAS model[12] to represent the Si(111)-(7×7) reconstruction. The major findings are that the activation energy for silicon-atom diffusion on the DAS surface is expected to be much higher than for the Binnig *et al.*[5] model and the corresponding rates orders of magnitude smaller. In addition, we find that diffusion patterns on the DAS surface are isotropic, in sharp contrast to the results obtained using the Binnig *et al.* model. Consequently, it is proposed that careful measurements of such quantities could lead to a more definitive evaluation of the structure of the Si(111)-(7×7) surface.

II. METHODS

For the Si(111)-(7×7) reconstructed surface, we employ the DAS model structure given by Takayanagi *et al.*[12] In this model, there are 19 silicon atoms per unit cell with dangling bonds. Of these, 12 are in the top layer (adatom

 0021-9606/91/096243-07$03.00

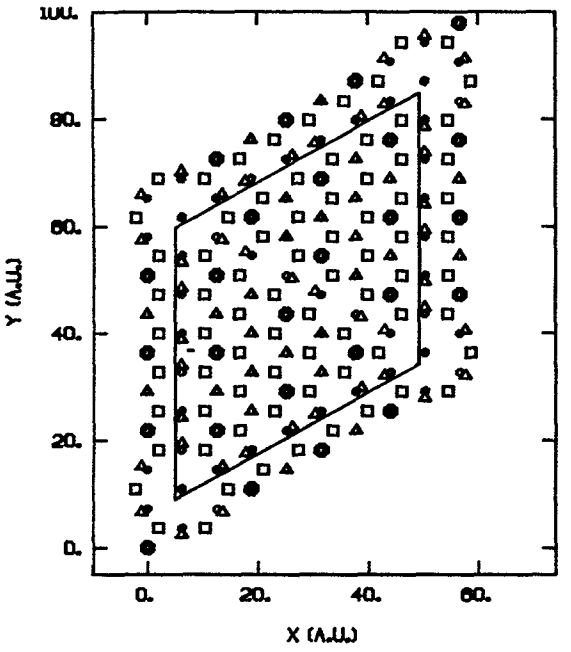

FIG. 1. A top view of the DAS model for the Si(111)-(7×7) reconstruction. The parallelogram defines the unit cell. For the sake of clarity, the origin of the parallelogram is arbitrarily chosen such that no atom lies on its boundary. Thus it may be seen that out of four atoms near the corner of the unit cell only one lies within the unit cell. Large circles denote top-layer atoms. Squares denote second layer atoms. Triangles and small circles represent the third and fourth layer atoms, respectively. The overlap of triangles, small circles, and large circles is also shown.

layer), 6 are in the second layer (stacking fault layer), and one is in the fourth layer. Figure 1 shows the relative positions of the atoms in the first four layers of the (7×7) unit cell. Figure 2 shows the 162 first and second layer atoms with

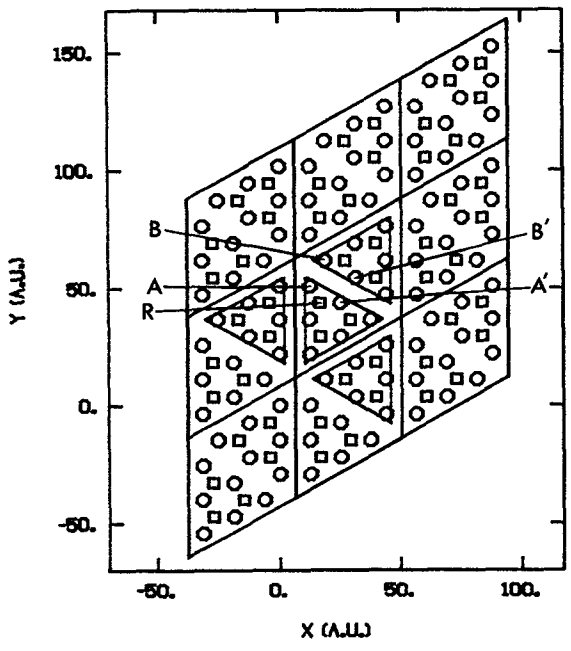

FIG. 2. A top view of atoms with dangling bonds in the first two layers of nine unit cells of the DAS surface. Circles and squares denote the first and second layer atoms, respectively.

dangling bonds contained in 9 adjacent unit cells on the (7×7) DAS surface.

To compute the silicon-atom diffusion rate on the DAS surface, we first calculate the rate at which silicon adatoms chemisorbed at site A (see Fig. 2) diffuse to other absorption sites on the surface. This is most easily done by calculating the root-mean-square displacement $\langle r^2(t)\rangle$ of silicon adatoms. This is given by

$$\langle r^2(t)\rangle = \sum_{i=1}^{N} [C_i(t) r_i^2(t)] \Big/ \sum_{i=1}^{N} [C_i(t)], \tag{1}$$

where t is the time, $C_i(t)$ is the concentration of diffusing adatoms at time t at the ith site which is at distance r_i from site A, and N is the total number of such sites considered. The root-mean-square displacement is directly related to the thermal diffusion coefficient D by

$$\langle r^2(t)\rangle = 2\alpha\, Dt, \tag{2}$$

where α is the dimensionality of the diffusion.

If the jump frequencies K_{ij} between sites i and j are known, then the time variation of the concentration of adatoms at site i is

$$\dot{C}_i(t) = \sum_{j=1}^{N}{}' [-K_{ij}C_i(t) + K_{ji}C_j(t)], \quad (i = 1,2,3,\ldots,N). \tag{3}$$

Equation (3) is based upon the assumptions that site-to-site jumps are first-order processes involving motion that is uncorrelated with previous jumps. The latter assumption will be reasonable if the characteristic time for diffusion, given by the inverse of K_{ij}, is much larger than the vibrational relaxation time, which may be on the order of 1000 vibrational periods. The values of the K_{ij} computed for the DAS surface and for the Binnig *et al.* surface[17] show that this condition is satisfied for these systems.

The required jump frequencies are obtained using the variational phase-space theory methods that were previously employed to obtain silicon-atom diffusion rates on the Binnig *et al.* surface.[17] In this method, the jump frequency is written as the ratio of the total flux crossing some dividing surface S_a that completely separates the diffusion sites to the total volume of phase-space corresponding to the adatom chemisorbed on the original site. That is,

$$K_{ij} = F\{\int_{S_a} I_{\text{out}} \exp[-\beta V_{\text{La}}]\exp[-\beta H']\mathbf{v}\cdot d\mathbf{S} \Big/ \int_{\Omega_a}\exp[-\beta V_{\text{La}}]\exp[-\beta H']d\Omega\}, \tag{4}$$

where

$$H' = H - V_{\text{La}}, \tag{5}$$

with H being the total system Hamiltonian and V_{La} the lattice–adatom interaction potential. $\mathbf{v}$ is the generalized velocity in the phase space of the system and

$$I_{\text{out}} = +1 \quad \text{for } \mathbf{v}\cdot d\mathbf{S} > 0 \tag{6}$$

and

$$= 0 \quad \text{otherwise.}$$

In Eq. (4), Ω_a is the total phase-space volume corresponding to a silicon adatom chemisorbed at the initial site and F is

a dynamical correction factor for recrossings of the dividing surface.

The ideal dividing surface would be such that trajectories cross once and only once in going from an adatom chemisorbed at the initial site to one chemisorbed at the final site. Under such conditions, the dynamical correction factor would be unity. For any other surface, the total flux across S_a will be an upper limit to the true classical rate. In the present method, the flux is minimized with respect to parameters contained in the definition of S_a. The factor F then introduces an appropriate correction for the remaining recrossing trajectories.

The integrals in Eq. (4) are evaluated using standard Monte Carlo procedures with importance sampling as described in Ref. 18. The Monte Carlo approximant for K_{ij} is

$$K_{ij} = [F/2w] \sum_j I_j'(S_a, w)|v_p|[P_0^{-1}] \Big/ \sum_j I_j'(\Omega_a)[P_0^{-1}]. \tag{7}$$

In Eq. (7), j refers to the jth accepted move in a canonical Markov walk, $P_0 = \exp[\beta V_{\rm La}]$, and $|v_p|$ is the magnitude of $\mathbf{v}\cdot\mathbf{dS}$, i.e., the magnitude of the component of the velocity of the adatom "perpendicular" to the dividing surface S_a. $I_j'(S_a, w)$ is an operator that has the value $+1$ if, by the jth move, the adatom is within the volume bounded by surfaces S_a and S_a', where S_a' is a surface very close and parallel to S_a at a distance w from S_a; otherwise $I_j'(S_a, w)$ is equal to zero. The operator $I_j'(\Omega_a)$ is equal to $+1$ if the jth move leads to a state such that the adatom is inside the volume Ω_a enclosed by the surface S_a. It is zero otherwise. The correction factor F for surface recrossings is obtained by the calculation of M trajectories starting from phase-space points (q,p) located between surfaces S_a and S_a' that occurred in the Markov walk. The correction factor is then given by

$$F = \sum_{j=1}^{M} I_j|v_p|_j[P_0^{-1}]_j \Big/ \sum_{j=1}^{M} |v_p|_j[P_0^{-1}]_j, \tag{8}$$

where I_j is unity if trajectory j does not recross S_a and maps properly into the product and reactant configuration space; otherwise, I_j is zero. The details for the execution of the Markov walk have been previously described.[17]

III. RESULTS AND DISCUSSION

The methods described in Sec. II were used to calculate jump frequencies, diffusion coefficients, and diffusion patterns on the DAS model of the Si(111)-(7×7) surface. To reduce the computational requirements, we have assumed the lattice atoms to be fixed in their equilibrium configuration. The effect of surface phonons are therefore not included in the present study. The expected magnitude of the error introduced by this omission is discussed below. The gas–lattice interaction potential is taken to be the same as that used in our study of silicon-atom diffusion on the Binnig *et al.*[5] model of the (7×7) reconstruction.[17] This potential assumes that pairwise-additive Lennard-Jones (12,6) interactions exist between all lattice atoms with dangling bonds and the silicon adatom. The well depth and equilibrium bond length parameters ϵ and r_0 are 2.515 eV and 4.0 a.u., respectively. The interaction between the adatom and a lattice atom without a dangling bond is obtained from the results of self-consistent field calculations at the 3-21G level.[17] The total interaction potential is the pairwise sum over all lattice sites contained in the first four layers of one (7×7) unit cell and the adjoining parts of all nearest-neighbor unit cells. The result of this summation is a net lattice–adatom binding energy of 2.31 eV. A detailed discussion of the accuracy of this potential and of the sensitivity of the diffusion results to various parameters in the potential has previously been given.[17]

A. Jump frequencies

The jump frequency K_{AB} of a silicon adatom between the sites denoted "A" and "B" in Fig. 2 has been computed using Eq. (7).

The region of interest for A→B diffusion is shown in Fig. 3. This figure shows the relative positions of all lattice atoms in the first two layers that have dangling bonds. Sites A and B are so indicated. A section of the dividing surface separating the reactant and product configuration space for the jump process is also shown. We take the dividing surface to be a right cylinder having a cross section in the surface plane (X–Y plane) as shown by the region DEFGHD in Fig. 3. The portion DEF is part of an ellipse with the major axis along FD of length FD = $2a$ and semiminor axis along AE of length AE = b. The region FGHD is a rectangle.

A partial minimization of K_{AB} with respect to the parameters defining the dividing surface has been carried out by direct calculation using Eq. (7). In this minimization, we have varied the side length FG over the range $0.5 \leqslant FG \leqslant 8.5$ a.u. with $b = 3.6$, 3.8, and 4.0 a.u. In all calculations, $a = 6.0$ a.u. and the

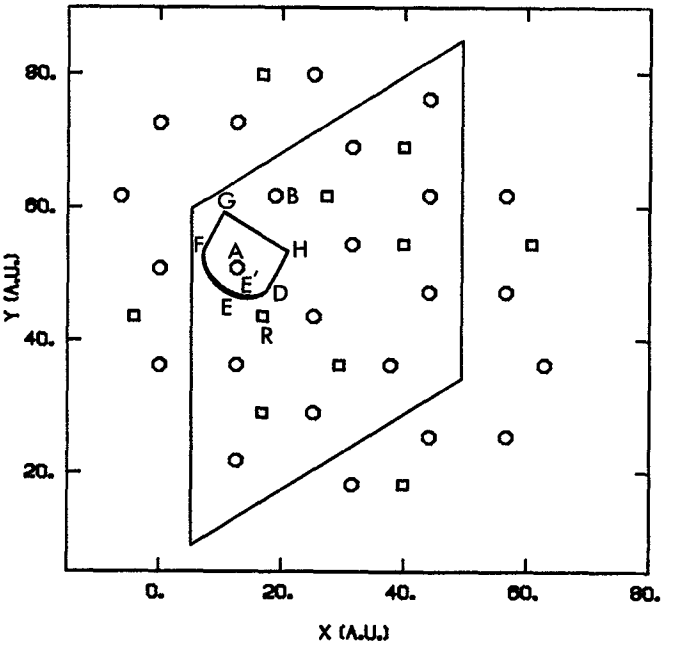

FIG. 3. A portion of Fig. 2 showing the region of interest for silicon-atom surface diffusion and the cross section of the dividing surface used in the variational calculations. The parallelogram denotes the unit cell. Circles and squares represent the atoms with dangling bonds in the first and second layers, respectively.

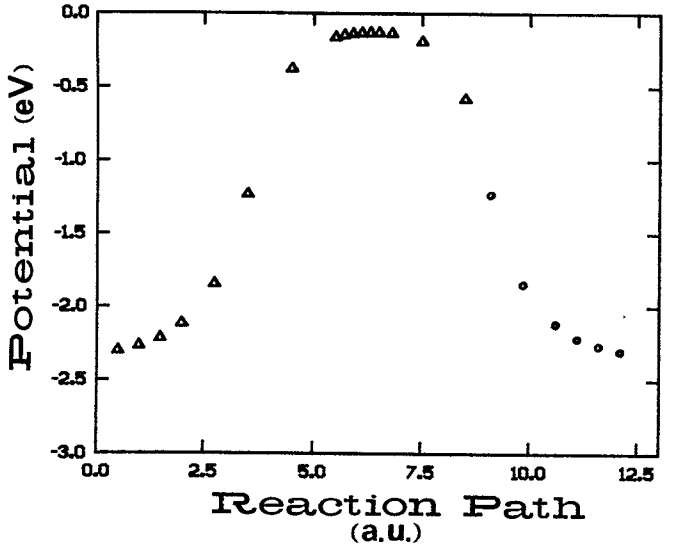

FIG. 4. Minimum-energy diffusion path for A→B jumps. The energy is given in eV. The triangles denote the data obtained in the variational calculations. The circles are extrapolated results based on symmetry considerations.

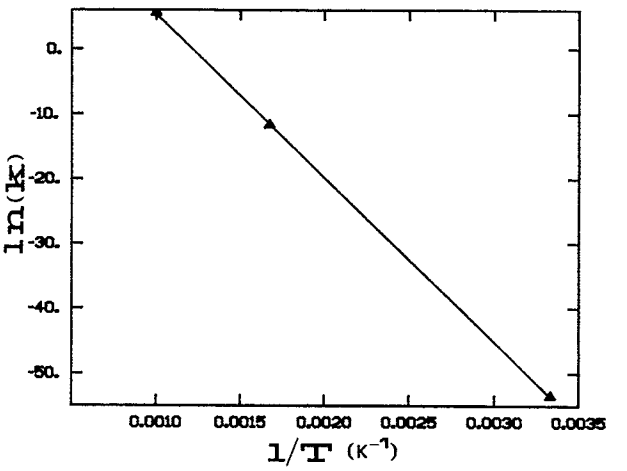

FIG. 5. Arrhenius plot of the A→B jump frequency.

surface S'_a, which defines the transition state for A→B diffusion, is taken to be parallel to GH. The calculated jump frequencies are found to be insensitive to b over the range $3.6 \leqslant b \leqslant 4.0$ a.u. This follows from the fact that the density of reactant phase space for b in the above range is very small. In Fig. 3, DEF corresponds to the dividing surface with $b = 4.0$ a.u. while DE'F is the dividing surface for $b = 3.6$ a.u. This result also suggests that the calculated jump frequency would be an insensitive function of the shape of the DEF boundary.

The minimum flux is obtained for a dividing surface that has GH lying along the perpendicular bisector of AB. Figure 4 shows the minimum-energy A→B diffusion path obtained by methods previously described by Raff *et al.*[18] The points correspond to the minimum potential-energy configuration observed in the Markov walk at dividing surfaces set at intervals along the reaction path. The abscissa values of the points in Fig. 4 correspond to the value of FG that defines the particular dividing surface. The barrier height for the A→B jump obtained from these studies is 2.18 eV. As can be seen, the location of the barrier maximum corresponds to GH lying along the AB bisector. That is, for this system, the minimum flux is obtained for a dividing surface that traverses the barrier maximum.

The correction factor F for surface recrossings has been obtained by explicit trajectory integrations starting from phase-space points lying in the transition-state region that were obtained in the Markov walk. The procedure is described in more detail in Ref. 17. In the present calculations, we have taken $M = 100$. The result is $F = 0.616$.

Minimized jump frequencies corrected for recrossings were computed at 300, 600, and 1000 K. The results are given in Table I. An Arrhenius plot of these data is shown in Fig. 5. The slope of the least-squares linear fit yields an activation energy of 2.18 eV, in excellent agreement with the results of the minimum-energy path calculations. The frequency factor obtained from the intercept of Fig. 5 is 2.07×10^{13} s^{-1}, which is significantly larger than that previously obtained for surface jumps between sites equivalent to A→R (see Figs. 2 and 3) on the Binnig *et al.*[5] model of the (7×7) reconstruction.[17]

TABLE I. Jump frequencies K_{AB} for A→B jumps and the diffusion coefficient D in cgs units as a function of the surface temperature T in degrees Kelvin.

T	K_{AB}	D
300.0	0.567×10^{-23}	0.341×10^{-37}
600.0	0.862×10^{-5}	0.519×10^{-19}
1000.0	0.253×10^{3}	0.151×10^{-11}

B. Diffusion coefficients

Silicon-adatom surface diffusion coefficients have been calculated at 300, 600, and 1000 K using Eqs. (1)–(3). In each of these calculations, the following assumptions are made:

(1) $K_{ij} = K_{ji}$.

(2) The A to R distance on the DAS surface is 8.5 a.u. We therefore assume that the A→R jump frequency is equal to that obtained in our previous calculations[17] for jumps of a similar distance. We show below that the diffusion coefficient is not sensitive to the actual value used for K_{AR}.

(3) Figure 2 shows that there are four types of jumps over a distance of 12.6 a.u. (a) A to B, (b) B to A, (c) A' to B', and (d) B' to A'. Symmetry considerations indicate that $K_{AB} = K_{BA}$. Likewise, we would expect $K_{A'B'} = K_{B'A'}$. The insensitivity of the jump frequency (see the previous section) to the nature of the DEF boundary shows that the presence of lattice site R does not significantly affect the value of the A→B jump frequency. If we neglect the presence of site R, symmetry arguments would indicate that $K_{AB} = K_{A'B'}$. We therefore assume that the A→B jump frequencies given in Table I may be used for all four types of jumps over a 12.6 a.u. distance.

(4) The K_{ij} for jumps over a distance greater than 12.6 a.u. are zero. The A–A' distance is 14.5 a.u. An inspection of the geometric arrangement of lattice sites in Figs. 2 and 3 shows that direct jumps from A to A' are not important. The diffusion to A' from A via site R would be very fast compared to the

direct jump rate. Consequently, neglect of direct, long-distance jumps is not expected to significantly affect the results for the overall diffusion coefficients.

We take the initial value of the $C_i(t=0)$ to be zero for all lattice atoms except site A. Solution of Eq. (3), coupled with Eq. (1), allows $\langle r^2(t)\rangle$ to be computed as a function of t. Figure 6 shows a typical result at 1000 K using $K_{ij} = 5.37\times10^4$ s^{-1} for jumps over an 8.5 a.u. distance.[17] Using Eq. (2), the diffusion coefficient may be extracted from the slope of the linear least-squares fit to the data in Fig. 6.

The results clearly show the existence of two distinct slopes. During the initial stages of diffusion between point P1 to P2, $\langle r^2(t)\rangle$ rises rapidly indicating a very large diffusion coefficient. After 3×10^{-4} s, the diffusion rate and the slope of the $\langle r^2(t)\rangle$ vs t plot decrease significantly. Over the range $0\leqslant t\leqslant$P2, surface diffusion is controlled by the A→R jump frequencies and equilibrium is quickly established over the lattice sites within one of the large triangular areas shown in Fig. 2. The diffusion coefficient for this process calculated from Eq. (2) and the part of plot between P1 and P2 is 3.7×10^{-11} cm^2/s. Diffusion between the triangular areas shown in Fig. 2 is controlled by the A→B jump frequencies which are much smaller than those for the shorter A→R jumps. Consequently, the smaller slope of the $\langle r^2(t)\rangle$ vs t plot seen at larger times essentially measures the rate of diffusion from one triangular area to another. This is the rate-controlling step in the diffusion process. The diffusion coefficients obtained from the long-time behavior of the system are given in Table I.

The rate-controlling diffusion coefficient for the system is very insensitive to the equilibration rate within one of the triangular areas, even at 1000 K. At lower temperatures, the relative duration of the P1–P2 portion of the $\langle r^2(t)\rangle$ curve would be even less than that seen in Fig. 6 due to the fact that the K_{AR}/K_{AB} ratio increases as the temperature decreases. This analysis is easily verified by some numerical calculations. Table II gives the calculated diffusion coefficients at 300, 600, and 1000 K for various assumed K_{AR}/K_{AB} ratios. The variations in D so obtained are all less than 7.3% even for infinite values of K_{AR}.

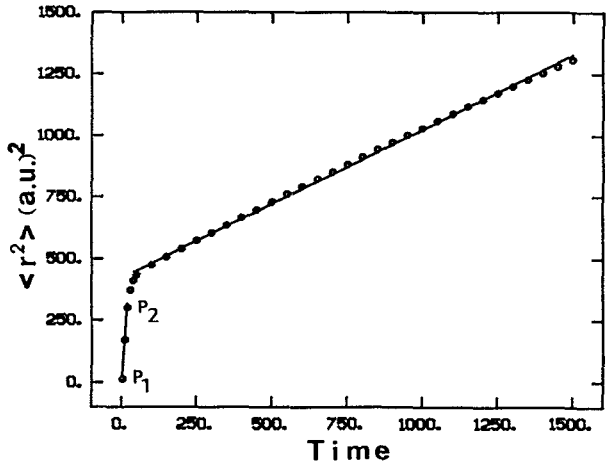

FIG. 6. $\langle r^2(t)\rangle$ as a function of time. r is given in a.u. and time in units of 3×10^{-6} s. $T = 1000$ K.

TABLE II. Diffusion coefficients D in cgs units as a function of jump frequencies.

T	K_{AR}/K_{AB}	D
300	200.0	0.351×10^{-37}
	500.0	0.334×10^{-37}
	3000.0	0.342×10^{-37}
	infinite	0.341×10^{-37}
600	200.0	0.558×10^{-19}
	500.0	0.529×10^{-19}
	3000.0	0.520×10^{-19}
	infinite	0.519×10^{-19}
1000	100.0	0.153×10^{-11}
	212.0	0.151×10^{-11}
	500.0	0.145×10^{-11}
	infinite	0.152×10^{-11}

If the K_{ij} for jumps over distances of 8.5 a.u. are assumed to be infinite, then instantaneous equilibration of the concentration of adatoms over all lattice sites within the triangular areas shown in Fig. 2 would be achieved. Under such conditions, the diffusion model can be simplified by considering each nine-atom triangular unit as a single "lattice site." Thus each (7×7) unit cell would have two such sites. Such a diffusion model for 49 unit cells in illustrated in Fig. 7. The nine unit cells enclosed in the parallelogram correspond to the those pictured in Fig. 2. In this model, diffusion is seen to be from a half-unit cell to another neighboring half-unit cell, of which there are three, symmetrically situated at 120° angles.

Equations (1)–(3) may be used to compute the diffusion coefficient for the two-site model shown in Fig. 7, provided the $C_i(t)$ are replaced with $C_i(t)/9$ and the K_{ij} with $3\times K_{ij}$. The first replacement is required to compensate for the fact that the

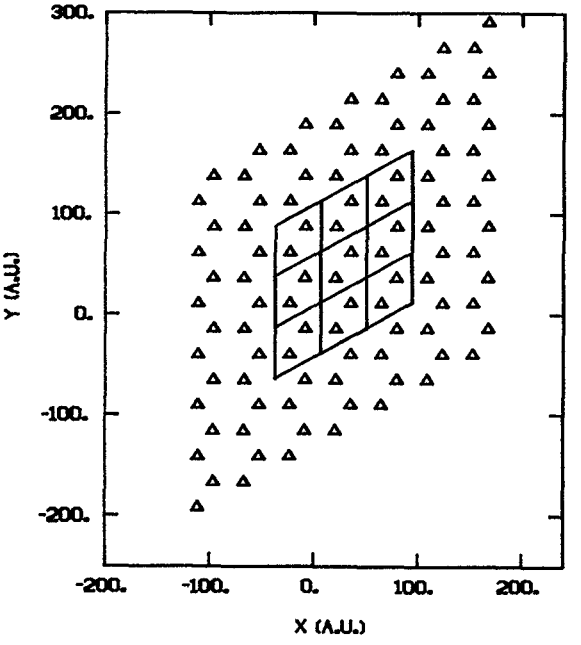

FIG. 7. The simplified diffusion model for 49 unit cells on the DAS surface. A triangle represents the triangular region shown in Fig. 2. Each triangle contains nine atoms with dangling bonds. The nine parallelograms enclose the region of the surface shown in Fig. 2.

total concentration in the triangular areas of Fig. 2 is nine times that at each lattice site at equilibrium. The second correction accounts for the fact that there are three A→B jumps that result in diffusion between triangular areas. The results labeled with an infinite K_{AR}/K_{AB} ratio in Table II have been obtained by this procedure.

Figure 8 shows an Arrhenius plot of the calculated thermal diffusion coefficients. The slope of the linear least-squares fit gives an activation energy of 2.18 eV. The pre-exponential factor obtained from the intercept is 0.124 cm^2/s.

In all of the above calculations, we have omitted consideration of surface motion. It has previously been shown[19-21] that the presence of surface phonons increases the surface diffusion rate. The classical diffusion rate is increased because the surface motion results in a smaller average diffusion distance. This, in turn, produces a decrease in the classical barrier to diffusion. The quantum mechanical tunneling rates are also increased primarily because of a narrowing of the barrier thickness through which tunneling must occur.

In the present case, the magnitude of surface phonon effects is expected to be small. Due to the large silicon-adatom mass, the tunneling contribution to the diffusion rate is negligible. In our previous studies of hydrogen-atom diffusion on unreconstructed Si(111) surfaces with partial hydrogen coverage,[19] we found a top to open-site diffusion barrier of 2.79 eV when surface phonon effects were omitted. The inclusion of surface motion reduced this barrier to 2.65 eV. For the present system, we expect the effect of surface motion on the classical diffusion barrier to be even smaller. This expectation is based on the shape of the barrier profile shown in Fig. 4. Because of the large diffusion distance (12.6 a.u.), the barrier is very flat in the transition-state region. Consequently, it seems unlikely that the small decrease in the average diffusion distance produced by surface phonon effects would result in a significant reduction in the barrier height. Nevertheless, some decrease is expected. Consequently, the values given for the diffusion coefficients in Tables I and II should be regarded as tight upper bounds to the values to be expected when full surface motion is included in the calculations.

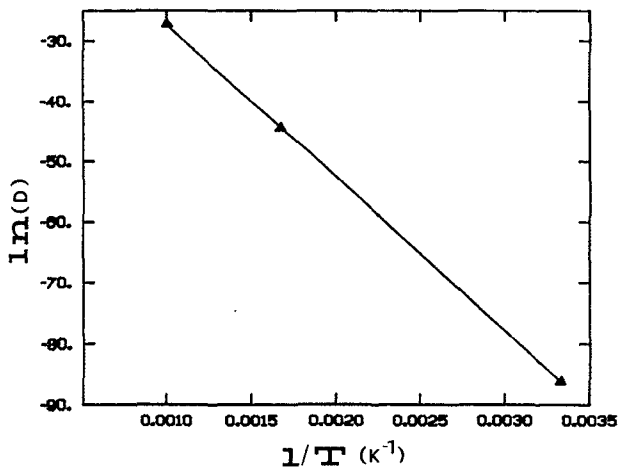

FIG. 8. Arrhenius plot for the diffusion coefficient. D is given in cgs units. T is in degrees Kelvin.

C. Comparison of diffusion on the DAS and Binnig surfaces

The magnitude and nature of silicon-atom surface diffusion on the DAS[12] and Binnig *et al.*[5] models of the Si(111)-(7×7) reconstruction are so different that it would appear that careful measurements of these quantities, if possible, would give a good indication of the extent to which each model accurately represents the experimental surface.

Due to the shorter jumps required on the Binnig *et al.*[5] surface, the diffusion rates are much larger than those obtained for the DAS model even with an identical interaction potential. Table III gives the ratio of the calculated diffusion coefficients for the two models. These vary from a factor of 32 at 1000 K to more than 9 orders of magnitude at 300 K. This is primarily the result of a much larger activation energy on the DAS surface (2.18 eV) compared to that for the Binnig surface (1.51 eV). The pre-exponential factors are also very different for the two surface models. We obtain 0.124 cm^2/s for the DAS surface compared to 0.002 15 cm^2/s on the Binnig model.

There have been several measurements of silicon-atom diffusion rates on Si(111) surfaces reported. Unfortunately, there is virtually no agreement between the results. Joyce *et al.*[22] obtain an activation energy in the range 1.73–2.52 eV based on their molecular beam experiments on SiH_4 pyrolysis. Farrow[23] carried out similar measurements and obtained E_a in the range 1.30–1.82 eV. Henderson and Helm[24] report a value of 1.04 eV. Abbink *et al.*[25] have obtained a value of 0.20 eV based on the results of direct deposition experiments in ultrahigh vacuum. The disparity in these data make it essentially impossible to draw any conclusions with regard to the extent to which the DAS and Binnig models accurately reflect the geometry of the experimental Si(111)-(7×7) surface.

In addition to differences in the magnitude of the diffusion rates, the diffusion patterns on the DAS and Binnig models are also very different. We have previously reported[17] that diffusion on the Binnig *et al.*[5] model is nonisotropic. Diffusion out of a given (7×7) unit cell occurs predominately at gateways located at three of the four corners of the unit cell. This results in a "directional diffusion coefficient"[17] that clearly shows the existence of preferential directions of silicon-adatom flow. In contrast, the symmetry of the model shown in Fig. 7 indicates that surface diffusion on the DAS surface will tend to be much more isotropic with no preferential directions for adatom flow. To date, there have been no measurements of such properties for silicon-atom surface diffusion.

TABLE III. Ratio of the silicon-atom diffusion coefficients calculated on the Binnig *et al.* model of the (7×7) reconstructed surface to those obtained with the DAS model as a function of temperature in degrees Kelvin.

T (K)	D(Binnig)[a]/D(DAS)[b]
300	2.5×10^9
600	9.3×10^3
1000	3.2×10^1

[a] Reference 17.
[b] Present calculations.

ACKNOWLEDGMENTS

We are indebted to Dr. Betsy M. Rice for discussions of various aspects of the variational phase-space theory calculations. P.M.A. would like to thank Dr. Ramesh Sharda and his family for their hospitality during the course of this work. We are pleased to acknowledge financial support from the Air Force Office of Scientific Research under Grant No. AFOSR-89-0085. P.M.A. expresses his thanks to Vikram University, Ujjain, India, for granting him leave to pursue this research.

[1] D. J. Chadi, R. S. Bauer, R. H. Williams, G. V. Hansson, R. Z. Bachrach, J. C. Mikkelsen, F. Houzay, G. M. Guechar, R. Pinchaux, and Y. Petroff, Phys. Rev. Lett. **44**, 799 (1980).
[2] D. J. Miller, D. Haneman, and L. W. Walker, Surf. Sci. **94**, 555 (1980).
[3] D. J. Miller and D. Haneman, Surf. Sci. **104**, L237 (1981).
[4] W. A. Harrison, Surf. Sci. **55**, 1 (1976).
[5] G. Binnig, H. Rohrer, C. Gerber, and E. Weibel, Phys. Rev. Lett. **50**, 120 (1983).
[6] M. Aono, R. Souda, C. Oshima, and Y. Ishizawa, Phys. Rev. Lett. **51**, 801 (1983).
[7] L. C. Synder, Surf. Sci. **140**, 101 (1984).
[8] P. A. Bennett, L. C. Feldman, Y. Kuk, E. G. McRae, and J. E. Rowe, Phys. Rev. B **28**, 3656 (1983).
[9] E. G. McRae, Phys. Rev. B **28**, 2305 (1983).
[10] F. J. Himpsel, Phys. Rev. B **27**, 7782 (1983).
[11] F. J. Himpsel and I. Batra, J. Vac. Sci. Technol. A **2**, 952 (1984).
[12] K. Takayanagi, Y. Tanishiro, M. Takahaski, H. Motoyoski, and K. Yagi, in Proceedings of the 10th International Congress on Electron Microscopy, Hamburg, 1982, Vol. 2, p. 285.
[13] R. M. Tromp and E. J. van Loenen, Surf. Sci. **155**, 441 (1985).
[14] R. M. Tromp, Surf. Sci. **155**, 432 (1985).
[15] T. Yamaguchi, Phys. Rev. B **30**, 1992 (1984).
[16] P. N. Keating, Phys. Rev. **145**, 637 (1966).
[17] P. M. Agrawal, D. L. Thompson, and L. M. Raff, J. Chem. Phys. **91**, 6463 (1989); **91**, 5021 (1989).
[18] L. M. Raff, I. NoorBatcha, and D. L. Thompson, J. Chem. Phys. **85**, 3081 (1986).
[19] B. M. Rice, L. M. Raff, and D. L. Thompson, J. Chem. Phys. **88**, 7221 (1988).
[20] S. M. Valone, A. F. Voter, and J. D. Doll, Surf. Sci. **155**, 687 (1985).
[21] R. Jacquet and W. H. Miller, J. Phys. Chem. **89**, 2139 (1985).
[22] B. A. Joyce, R. R. Bradley, and G. R. Booker, Philos. Mag. **15**, 1167 (1967).
[23] R. F. C. Farrow, J. Electrochem. Soc. **121**, 899 (1974).
[24] R. C. Henderson and R. F. Helm, Surf. Sci. **30**, 310 (1972).
[25] H. C. Abbink, R. M. Broudy, and G. P. McCarthy, J. Appl. Phys. **39**, 4673 (1968).